nature chemistry

ARTICLES

https://doi.org/10.1038/s41557-018-0113-9

Isoreticular two-dimensional magnetic coordination polymers prepared through pre-synthetic ligand functionalization

J. López-Cabrelles[1,8], S. Mañas-Valero[1,8], I. J. Vitórica-Yrezábal[2], P. J. Bereciartua[3,7], J. A. Rodríguez-Velamazán[4], J. C. Waerenborgh[5], B. J. C. Vieira[5], D. Davidovikj[6], P. G. Steeneken[6], H. S. J. van der Zant[6], G. Mínguez Espallargas[1*] and E. Coronado[1*]

Chemical functionalization is a powerful approach to tailor the physical and chemical properties of two-dimensional (2D) materials, increase their processability and stability, tune their functionalities and, even, create new 2D materials. This is typically achieved through post-synthetic functionalization by anchoring molecules on the surface of an exfoliated 2D crystal, but it inevitably alters the long-range structural order of the material. Here we present a pre-synthetic approach that allows the isolation of crystalline, robust and magnetic functionalized monolayers of coordination polymers. A series of five isostructural layered magnetic coordination polymers based on Fe(II) centres and different benzimidazole derivatives (bearing a Cl, H, CH_3, Br or NH_2 side group) were first prepared. On mechanical exfoliation, 2D materials are obtained that retain their long-range structural order and exhibit good mechanical and magnetic properties. This combination, together with the possibility to functionalize their surface at will, makes them good candidates to explore magnetism in the 2D limit and to fabricate mechanical resonators for selective gas sensing.

Since the isolation of graphene, there has been an explosion in the search for other atomically thin layers[1]. Most of these 2D materials are layered inorganic materials that, in bulk, show stacked structures with weak van der Waals interactions between adjacent sheets, but with strong covalent bonding within each sheet. These materials exhibit a wide range of physical properties including insulators (h-BN)[2], semiconductors (1T-ZrS_2, 2H-MoS_2 or black phosphorous)[3–5], metals (1T-MoS_2)[6] and superconductors (Mo_2C, 2H-$NbSe_2$ or 2H-TaS_2)[7–9]. However, 2D magnetic materials (such as V_5S_8, $FePS_3$, $Cr_2Ge_2Te_3$ or CrI_3)[10–13] have remained elusive until recently due to their instability under ambient conditions and the difficulty to experimentally detect magnetism in the 2D limit. In fact, this challenging issue has only been achieved so far in the most favourable case (the Ising ferromagnet)[13].

Recently, a new and less explored field has emerged with 2D organic polymers (including covalent organic frameworks (COFs) and conjugated aromatic polymers (CAPs))[14,15] and 2D coordination polymers (enclosing coordination polymers (CPs) and metal–organic frameworks (MOFs))[16], which have been used for membranes[17], gas separation[18], electronics[19] and photoluminescence[20]. Owing to the fragility of the starting crystals, there are only a few examples that can be exfoliated micromechanically (and with limited lateral dimensions[15,21]), and liquid exfoliation is the most common methodology[17,22]. This prevents application of these exfoliated materials in areas where high-quality layers are required (nanoelectronics, for example), and their most recent uses are in the fields of catalysis[23] and membranes[24].

A rising interest in the field of 2D materials resides in their covalent functionalization, because surface engineering can lead to the rational modification of the surface properties (hydrophobicity, adhesivity or wettability, among others) or electronic properties of the layers[25,26]. As the surface modifications are generally performed following a post-synthetic method, high rates of surface functionalization are often challenging due to the poor reactivity and solubility of the inorganic surfaces[27]. Therefore, the molecules are anchored to the surface in a random way, leading to a defective and incomplete functionalization of the layered material. An alternative strategy for chemical surface modification is the pre-synthetic method, where the bulk layered material is chemically modified before exfoliation. This approach, which is infeasible in 2D inorganic materials, can be easily achieved in 2D coordination polymers due to the molecular composition of these compounds. Thus, through a rational choice of the functional substituent of the organic ligand, it is possible to achieve a periodically ordered decoration of the 2D coordination network, that is, a defect-free functionalized 2D material (Fig. 1).

Here, we present a new family of layered coordination polymers (LCPs), **MUV-1-X** (MUV = Material of the University of Valencia), with the general formula $[Fe(bimX)_2]$ (HbimX = benzimidazole functionalized in the 5-position with X = H, Cl, Br, CH_3 or NH_2), which exhibit cooperative magnetism and are robust enough to be micromechanically exfoliated down to the monolayer, while preserving their crystallinity. The pre-synthetic modification of the materials through a convenient choice of the organic substituent gives rise to a surface tunability ranging from hydrophilic to

[1]Instituto de Ciencia Molecular (ICMol), Universitat de València, Paterna, Spain. [2]School of Chemistry, University of Manchester, Manchester, UK. [3]Instituto de Tecnología Química (UPV-CSIC), Universitat Politècnica de València–Consejo Superior de Investigaciones Científicas, Valencia, Spain. [4]Institut Laue-Langevin, Grenoble , France. [5]Centro de Ciências e Tecnologias Nucleares, Instituto Superior Técnico, Universidade de Lisboa, Bobadela, Portugal. [6]Kavli Institute of Nanoscience, Delft University of Technology, Delft, The Netherlands. [7]Present address: Deutsches Elektronen-Synchrotron (DESY), Hamburg, Germany. [8]These authors contributed equally to this work: J. López-Cabrelles, S. Mañas-Valero. *e-mail: Guillermo.Minguez@uv.es; Eugenio.Coronado@uv.es

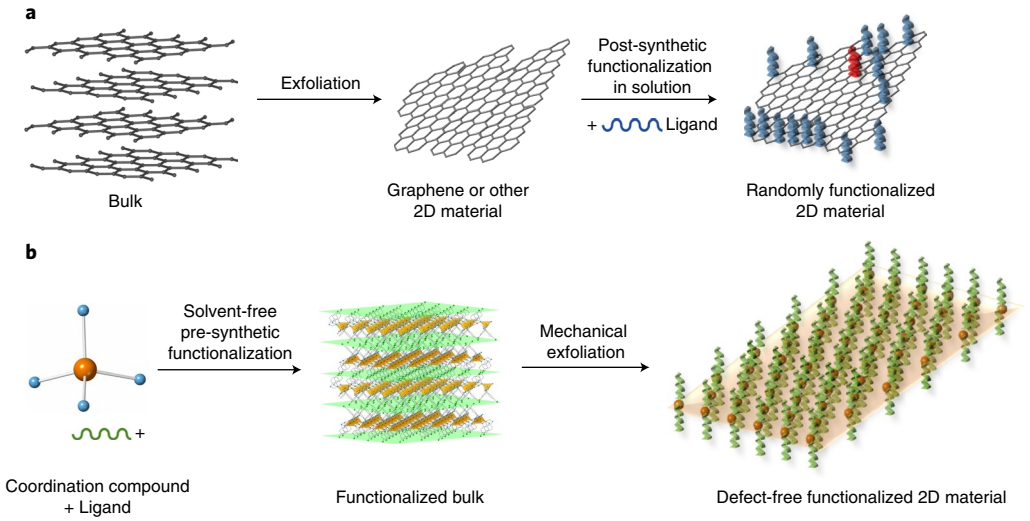

Fig. 1 | Schematic representation of post-synthetic covalent functionalization versus the pre-synthetic functionalization used here. a, Commonly used strategy to functionalize 2D (inorganic) materials, consisting of two steps: (1) mechanical or liquid exfoliation of the bulk material, then (2) functionalization in solution of the exfoliated material, yielding a random distribution of the functional groups, represented in blue. This route can also produce ligand modifications, represented with a colour change from blue to red. **b**, Pre-synthetic functionalization, in which the functionalized bulk is first obtained before being mechanically exfoliated, thus yielding a quasi-perfect array of unaltered functional groups attached to the surface.

hydrophobic, albeit maintaining the inner physical property (their magnetic order) in all the derivatives of the family.

Results

Synthesis and characterization of the LCPs. The solvent-free reaction of 5-chlorobenzimidazole (HbimCl) and ferrocene, adapting a previously described method for the preparation of iron azolates[28], yields large laminar colourless crystals with the formula $[Fe(bimCl)_2]$ (abbreviated as **MUV-1-Cl**), consisting of distorted tetrahedral Fe^{II} centres connected by 5-chlorobenzimidazolate bridges (Fig. 2a,b), forming a neutral LCP extending in the *a*–*b* plane. These layers interact weakly with each other through van der Waals interactions (Cl···Cl interactions). The compound is related to the diamagnetic Zn analogue $[Zn(bimH)_2]$, which was obtained via decomposition of a 3D MOF[17]. In these atomically thin layers, the Fe^{II} atoms are located in the inner part of the layers, whereas the Cl substituents are positioned at the surface (Fig. 2a), thus playing an active role in the chemical behaviour of the molecular interface. A close-up view with scanning electron microscopy (SEM) evidences the layered structure of **MUV-1-Cl** as the stacking of multiple sheets (Fig. 2c), with a typical size of ~400 μm, the purity of which was confirmed by powder X-ray diffraction (Supplementary Fig. 8). Room temperature infrared and Raman spectra present coincident peaks, indicating a non-centrosymmetric structure (Supplementary Fig. 40). Furthermore, room-temperature Mössbauer spectra consist of two doublets with the same relative area for Fe^{II}, indicating the presence of two different Fe^{II} sites with the same multiplicity (Supplementary Fig. 12). These features are consistent with space group *C*2, although the presence of a racemic mixture causes a better refinement of the single-crystal X-ray data in the *C*2/*c* space group. This is related to the weak interlayer interactions, which prevent long-range order in the *c* direction, but which is advantageous for exfoliation.

The short pathway between the iron centres, provided by the 5-chlorobenzimidazolate bridges, facilitates the presence of magnetic exchange in **MUV-1-Cl**, as evidenced in the plot of the molar magnetic susceptibility (χ_m) as a function of temperature in Fig. 2d (Supplementary Section 5.2). The χ_m versus *T* curve exhibits a broad maximum at 30.0 K and a sharp peak at ~20 K. In the plot of $\chi_m T$ versus *T*, a $\chi_m T$ value of 2.94 emu mol^{-1} K is observed at room temperature, in agreement with that expected for a high-spin Fe^{II}, $S=2$ (3.0 emu mol^{-1} K, where $g=2.0$), which decreases on cooling to 20 K (Supplementary Fig. 17). The behaviour in this region indicates the presence of dominant antiferromagnetic (AF) exchange coupling between the Fe^{II} centres, confirmed by a negative Curie-Weiss temperature, $\theta=-80.6$ K (Supplementary Fig. 16). These data can be quantitatively reproduced using a model for a quadratic-layer Heisenberg antiferromagnet[29] with $S=2$ $\left(H=-\sum_{i,j} JS_i \cdot S_j\right)$ (Fig. 2d and Supplementary Fig. 15). The resulting exchange parameter is $J=-22.9$ cm^{-1}. The abrupt increase in both χ_m and $\chi_m T$ suggests the occurrence of a magnetic transition towards a canted spin structure below the Néel temperature (T_N) of 20 K. The presence of an out-of-phase susceptibility signal below 20 K in the alternating current (a.c.) measurements confirms this kind of magnetic order (Fig. 2e and Supplementary Fig. 18). Powder neutron diffraction patterns collected at 1.8 K and 30 K, that is, below and above the ordering temperature (Supplementary Section 5.1), provide a further support on the AF ordering in this material. Still, in the present case these measurements are unable to detect the presence of spin canting, which is below the limit of detection of these measurements (Supplementary Section 5.1), mainly due to the small value of the ferromagnetic component resulting from canting, as deduced from susceptibility measurements.

From bulk crystals to the 2D limit. The layered nature of **MUV-1-Cl** and the absence of strong intermolecular interactions between adjacent layers prompted us to explore the possibility of mechanically exfoliating this material by the so-called Scotch-tape method, a conventional approach usually employed for graphene and other 2D materials, but rather rare in coordination polymers due to the fragile nature of the crystals[21]. The advantage of this dry method over liquid exfoliation is the potential of achieving of atomically thin layers with high crystallinity and larger lateral sizes.

Bulk crystals of **MUV-1-Cl** were exfoliated using a plastic tape (Ultron Systems) and deposited onto a silicon substrate with 285 nm of thermally grown SiO_2. As a result, a plethora of flakes with well-defined rectangular shapes (lateral dimensions of >1 μm) and different thicknesses (ranging from a single layer up to hundreds of nanometres) were obtained, as can be clearly seen by optical and atomic force (AFM) microscopies (Supplementary Figs. 22–28),

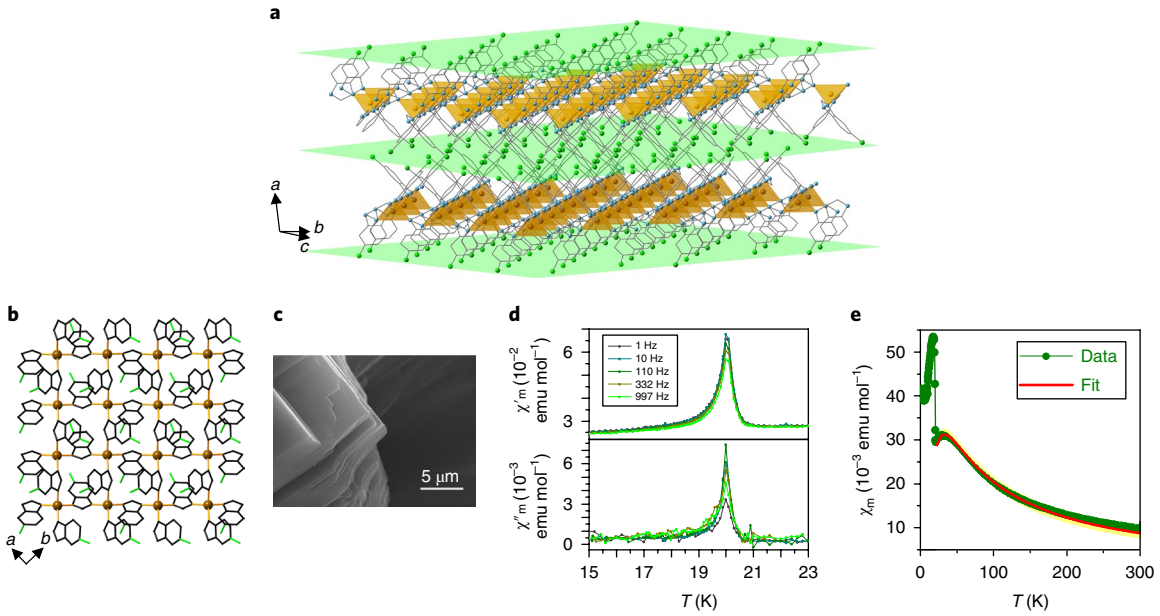

Fig. 2 | Bulk characterization of MUV-1-Cl. a, Layered structure of **MUV-1-Cl** showing the Cl atoms located at the surface of the layers, represented as green planes. Iron centres are shown in orange (polyhedral representation), nitrogen atoms in blue, carbon atoms in black and chlorine atoms in green. Hydrogen atoms have been omitted for clarity. **b**, Structure of a single layer of **MUV-1-Cl** viewed along the *c* axis (*a*–*b* plane). Colour code as in **a**. **c**, SEM image of the bulk material, clearly showing the layered structure. **d**, Temperature dependence of the in-phase (top) and out-of-phase (bottom) dynamic a.c. susceptibility of **MUV-1-Cl** measured at different frequencies. **e**, Thermal dependence of magnetic susceptibility in the temperature range 2–300 K. The data have been fitted (red line) following a Lines expansion for a quadratic-layer Heisenberg antiferromagnet with $S=2$ (ref. [29]). The yellow line represents the prediction bands with a confidence interval of 95%.

thus being air-stable. This contrasts with the lower-quality nanosheets obtained in a Zn analogue compound by liquid exfoliation[17]. A monolayer of dimensions $4\times1.5\,\mu m^2$ was isolated (Fig. 3a and Supplementary Section 6.2). The crystallinity, chemical composition and integrity of the exfoliated flakes were confirmed by transmission electron microscopy (TEM) and Raman studies on specimens of different thicknesses (Figs. 3b,d and Supplementary Section 6). To the best of our knowledge, this is the first time that selected-area electron diffraction (SAED) patterns have been obtained in a top-down micromechanically exfoliated LCP (Fig. 3d), and previously this has only been achieved with inorganic materials, mainly transition metal dichalcogenides[30,31]. There are some features that could be associated with diffuse scattering, resulting from the presence of a modulated commensurate structure in the bulk material (Supporting Sections 2 and 6.4). The indexation of these patterns indicates that they correspond to zone axis [0 0 1], confirming that the exfoliated flakes consist of one or several layers whose stacking along the *c* axis forms the original bulk material. The close resemblance between the experimental and simulated patterns (Fig. 3d and Supplementary Section 6.4) provides further evidence of this. Moreover, the well-defined Bragg peaks observed in the SAED patterns suggest that the exfoliation process does not damage the structure of the LCP, and the obtained flakes retain the crystallinity of the bulk material. Some of the SAED patterns were obtained from layers as thin as 20 nm—a notable result given the molecular nature of the material. We did not observe any thickness dependence of the unit cell or Raman peaks shift compared to the bulk counterparts.

The magnetic order of the atomically thin layers deposited in a silicon substrate was inspected by magnetic force microscopy at low temperatures (LT-MFM) in a dual-pass mode configured with a phase locked loop (PLL) feedback on the cantilever oscillation (Supplementary Section 6.5). In this configuration, the magnetic signal is related to the frequency shift (Δf) in such a way that an attractive tip–sample interaction is characterized by $\Delta f<0$ (red contrast), and a repulsive tip–sample interaction is characterized by $\Delta f>0$ (blue contrast)[32]. For simplicity for the comparison of magnetic images, in this work we defined the frequency shift to be 0 (green contrast) in the silicon substrate[33]. Below the order temperature, the flakes are imaged with a smoothly red contrast, indicative of an attractive tip–sample interaction, which disappears at temperatures above T_N (Fig. 3c), in agreement with a transition from a canted AF structure to a paramagnetic phase. In addition, as expected from the magnetic structure of the material (weak ferromagnet due to an AF canted structure), this contrast is very weak and furthermore it remains unaffected by the reversal of an applied in-plane external field (from +2 T to −2 T). Hence, from these measurements we cannot conclude that the signal has a pure magnetic component as it may also be influenced by other forces such as electrostatic ones. Low-temperature nano-magneto optical Kerr effect measurements and Kelvin-probe microscopy on individual sheets will be performed in the future to obtain further information on this issue.

Surface modification. Surface engineering is a demanding challenge in 2D materials because it permits the surface chemistry to be purposefully tuned (modifying, for example, the hydrophobicity/hydrophilicity), and subsequently enables the use of these systems at an industrial and technologically relevant scale. However, many of the reported processes to modify the surfaces of 2D materials lead to defective materials with altered electronic or magnetic properties[34], because they generally involve post-synthetic methods. To circumvent these problems, the pre-synthetic strategy we present enables modification of the surface properties of **MUV-1-Cl** with retention of the physical properties (magnetism). As a proof of concept we replaced (by chemical design) the substituent in the fifth position (Cl in **MUV-1-Cl**) with different groups such as CH_3 (**MUV-1-CH_3**), H (**MUV-1-H**), Br (**MUV-1-Br**) and NH_2 (**MUV-1-NH_2**), thus tuning the behaviour of the surface in contact with water,

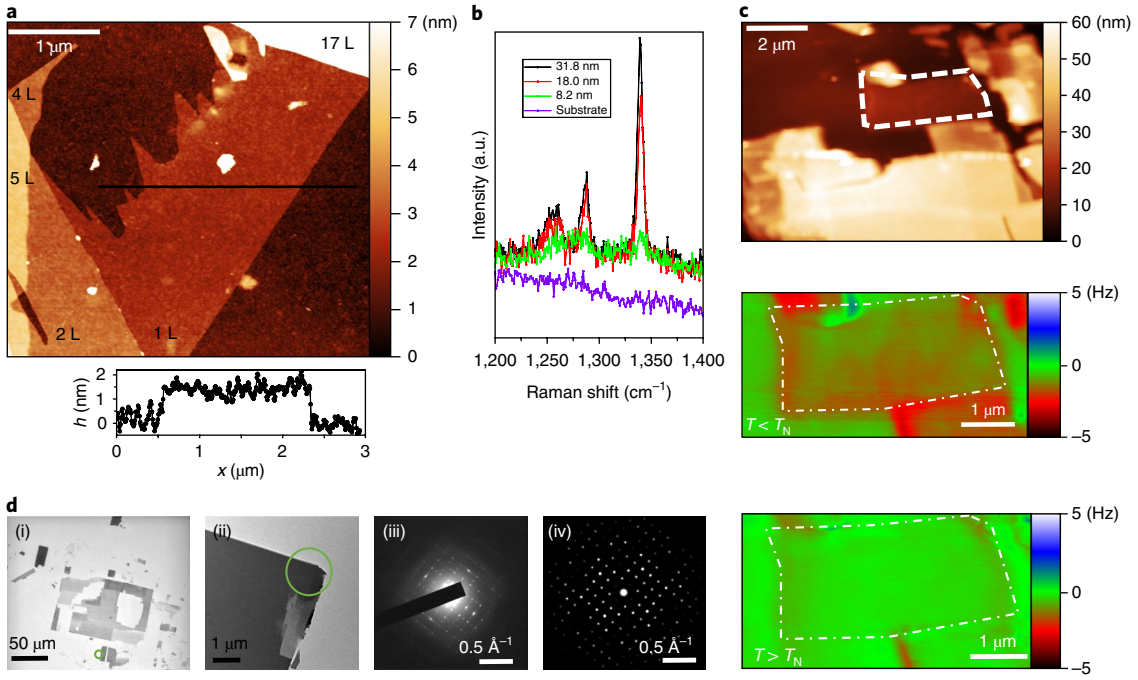

Fig. 3 | Atomically thin layers of MUV-1-Cl. a, AFM image and height profile of a flake of **MUV-1-Cl** (see Supporting Section 6.2 for further information). Different numbers of exfoliated layers (L) are indicated. **b**, Raman spectra for **MUV-1-Cl** flakes with different thicknesses. **c**, MFM measurements of a 5.7-nm-thick flake of **MUV-1-Cl**. Top: general topography image of the selected region with the flake highlighted by a dashed white line; middle and bottom: MFM images of the flake (highlighted by dot–dashed white lines) showing the difference in frequency shift below (middle) and above (bottom) T_N. Note the change in colour contrast below T_N, which indicates an attractive tip–sample interaction in the ordered state that disappears at temperatures above T_N. See Supplementary Section 6.5 for further information. **d**, (i) Low-magnification TEM image for **MUV-1-Cl** flakes, where darker grey areas are associated with thicker flakes; (ii–iv) selected area (enclosed by a green circle on the TEM image in (ii)) for which the experimental SAED pattern was obtained that corresponds to the [0 0 1] zone axis (iii), and which is in very good agreement with the simulated SAED pattern (iv).

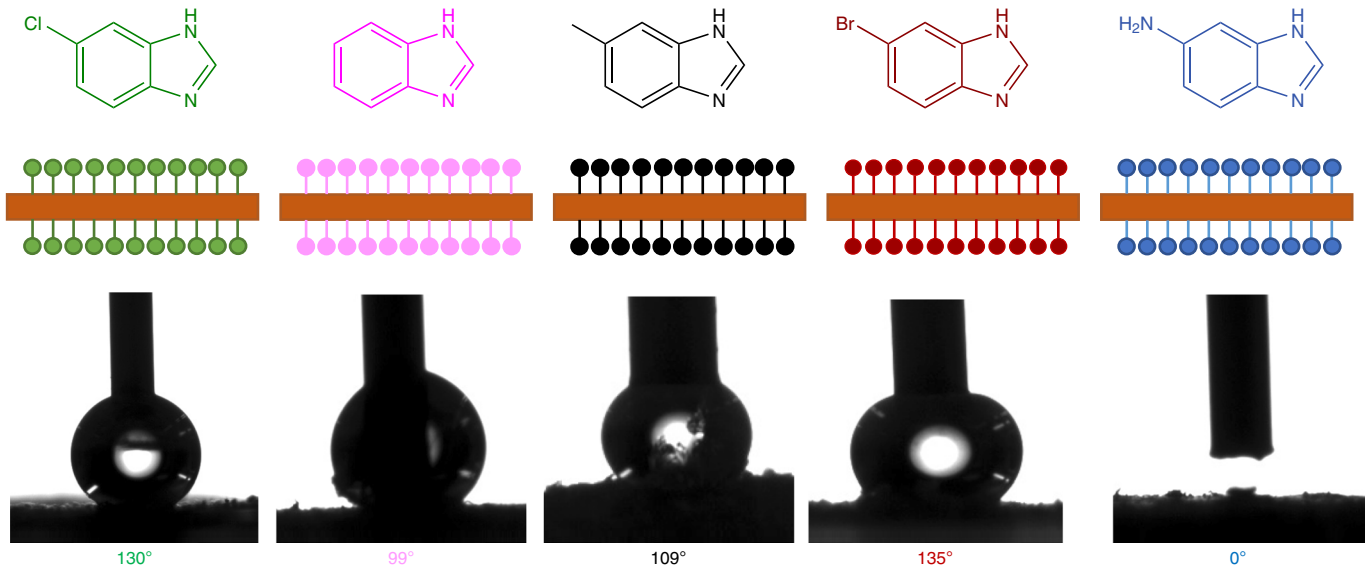

Fig. 4 | Surface modification in MUV-1-X. Atoms at the surface of **MUV-1-X** can be changed by chemical design (X = Cl, H, CH_3, Br, NH_2) in a pre-synthetic manner to obtain different surface behaviours that change the water contact angle. The structure of each derivatized ligand is shown (top) with a schematic representation of each functionalized 2D layer (middle) and a picture of a water droplet deposited on each surface (bottom), from which the contact angles are measured. No changes in the magnetic properties are observed following chemical modification (Supplementary Section 5).

from hydrophobicity values for the contact angle to hydrophilicity (Fig. 4). Alkane groups (H, CH_3) present contact angles of 99° and 109°, respectively (moderate hydrophobic behaviour). The inclusion of halide substituents causes an increase in the contact angles (130° and 135° for Cl and Br, respectively), thus showing an increase in hydrophobic character. In contrast, inclusion of the amino group (NH_2) causes a decrease of the contact angle to 0°, indicating super-hydrophilic properties.

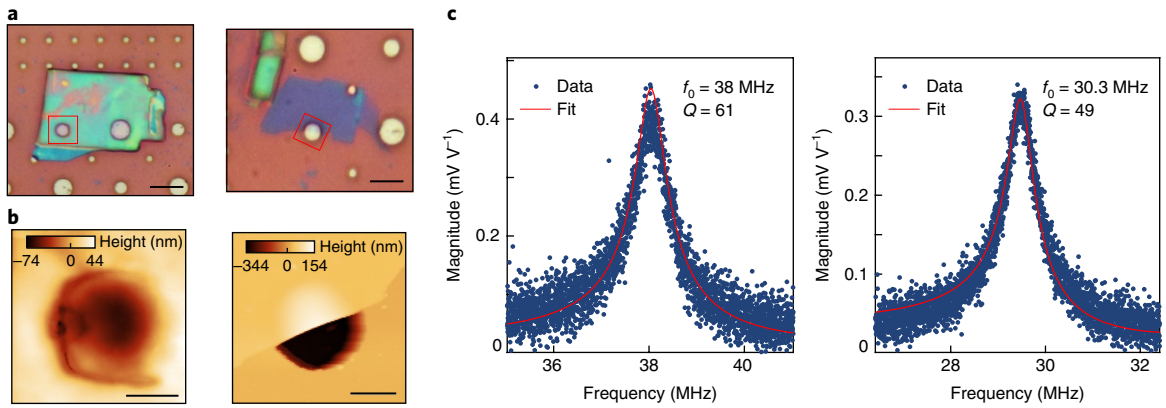

Fig. 5 | MUV-1-Cl suspended membranes. a, Optical images of two **MUV-1-Cl** flakes transferred on top of circular cavities on a Si/SiO_2 substrate. Scale bars, 5 μm. Left: flake with height of 74 nm; right: flake with height of 20 nm. Red boxes indicate regions where AFM has been measured. **b**, AFM images of the two drums taken in the area enclosed by red boxes in **a**. Scale bars, 1 μm. Left: drum corresponding to the flake with 74 nm height in **a** (left); right: drum corresponding to the flake with 20 nm height shown **a** (right). **c**, Two frequency-domain measurements on two different nanomechanical resonators made of **MUV-1-Cl**, with thicknesses of 70–80 nm. These are similar to those in **a** and **b**. The extracted resonance frequencies and *Q* factors of the two resonators are shown.

The five different ligands successfully employed already demonstrate large tunability, although we can anticipate that one of the possible limitations of this approach relies on the use of larger substituents that can interfere with the formation of the crystalline layered structure. However, preliminary results indicate that bulkier groups of up to three non-H atoms can also be incorporated with this approach, although further studies are ongoing.

The structural and magnetic properties of all these compounds were characterized by X-ray diffraction, magnetic susceptibility measurements, Mössbauer and Raman spectroscopies, SEM and TEM (see Supplementary Information). Remarkably, the magnetic properties of the entire **MUV-1-X** family remain unaltered with the different surface modifications, as can be seen in Supplementary Table 4 and Supplementary Section 5.2. In addition, all members of the **MUV-1-X** family have been exfoliated successfully by mechanical methods, and are characterized in detail as **MUV-1-Cl** (Supplementary Section 6).

The ability to tailor the functionality of **MUV-1-X**, combined with its mechanical resonant readout, makes it attractive for sensing applications, because the resonance frequency and quality (*Q*) factor of these suspended membranes are expected to depend strongly on the mass and adhesion of captured molecules. To demonstrate this concept, we exfoliated and transferred thin flakes of **MUV-1-Cl** on top of a Si/SiO_2 substrate with prepatterned circular cavities. Figure 5a presents optical images of two exemplary flakes transferred on top of cavities, forming suspended nanodrums. AFM images of the drums (areas enclosed by red boxes in Fig. 5a) are shown in Fig. 5b. The device shown in the left panel of Fig. 5a,b is 74 nm thick, whereas the thickness of the one in the right panel is 20 nm thick. Figure 5c,d shows the mechanical frequency response of two **MUV-1-Cl** nanodrums (thicknesses of 70–80 nm). The measurements were performed in vacuum using a laser interferometry set-up, as described in the Methods. The resonance frequencies of the drums are 38 MHz and 30.3 MHz, with *Q* factors in the range 45–65. This variation may result from a combination of different thicknesses and geometries of the drums. The *Q* factors are comparable to those reported in nanomechanical resonators made of graphene and other 2D materials[35,36]. The lower *Q* factors may be due to viscoelastic damping in this polymer material. Because of the large diameter-to-thickness ratio, the resonance frequencies of these nanodrums are mainly determined by the bending rigidity of the material. For the given resonance frequencies and geometry of the drums, we thus estimate the Young's modulus of **MUV-1-Cl** to be 3–7 GPa, which is almost three orders of magnitude lower than that of graphene and similar to that previously reported for a LCP measured by AFM nanoindentation[37,38]. The results show that these polymer resonators, despite their low Young's modulus and potential viscous damping mechanisms, have surprisingly high *Q* factors and resonance frequencies, which are comparable to graphene membranes. In combination with their low weight and tunable functionalization, these materials can be used to create future platforms for resonance-based sensing.

Discussion

In this Article we have presented a general strategy for the synthesis of crystalline LCPs exhibiting magnetic order, and provide an unconventional route to tune at will the surface chemistry of the individual layers. In particular, by using different ligands, we have obtained a new family of LCPs denoted **MUV-1-X** (X = Cl, Br, H, CH_3 or NH_2), with surface properties ranging from hydrophobic to hydrophilic, that retain their magnetic properties under the different surface modifications. Interestingly, and in contrast with most reported MOFs, large crystals of these coordination polymers have been grown using a solvent-free synthesis. Such a possibility together with the layered nature of these materials and the very weak van der Waals forces between the layers have permitted the isolation of micrometre sized atomically thin flakes down to the monolayer by mechanical and dry exfoliation methods. The high crystallinity, integrity and chemical composition of these mechanically exfoliated layers has been confirmed by TEM and Raman studies on LCPs of different thicknesses.

On the other hand, and in contrast to what happens in the few examples of reported 2D ferromagnets based on solid-state chemistry[13], which have been shown to be highly unstable in open air, this coordination chemistry approach has afforded the isolation of robust 2D magnetic materials. This robustness—unusual for 2D coordination polymers—has also enabled us to study the mechanical properties of these materials. We believe that these 2D magnetic coordination polymers are promising for the preparation of high-quality resonators, which in turn makes them of potential interest as components in nanodevices. These findings point to the possible integration and application of 2D coordination polymers more generally in different technological areas such as nanoelectronics, coatings, molecular sensing or mechanical magnetic membranes. It also brings new candidates for the study of magnetism and phase transitions in the 2D limit. Finally, the variation of wettability opens the

possibility of creating complex stacked structures, where the interface would determine the formation of a heterostructure.

The fact that the pre-synthetic functionalization described here leads to defect-free ligand decoration of the monolayer may allow the combination of this magnetic 2D material with superconductors or graphene. We hope that this will lead to the preparation of materials in which unconventional physical phenomena might be present, such as Majorana fermions or photomagnon couplings.

Methods

Synthesis of MUV-1-X. Ferrocene (30 mg, 0.16 mmol) and benzimidazole (or derivates) (0.34 mmol) were combined and sealed under vacuum in a layering tube (4 mm diameter). The mixture was heated at 250 °C for 3 days to obtain crystals suitable for X-ray single-crystal diffraction. The product was allowed to cool to room temperature, and the layering tube was then opened. The unreacted precursors were extracted with acetonitrile and benzene, and the product was isolated as colourless crystals (yield 80%). Phase purity was established by X-ray powder diffraction. Energy-dispersive X-ray analysis of **MUV-1-Cl** from SEM and TEM show in both cases a 70:30 ratio for Cl:Fe.

X-ray structural studies. X-ray data for compounds **MUV-1-H** and **MUV-1-Cl** were collected at a temperature of 100 K using synchrotron radiation at single-crystal X-ray diffraction beamline I19 at Diamond Light Source, equipped with a Pilatus 2M detector and an Oxford Cryosystems nitrogen flow gas system. Data were measured using the GDA suite of programs. X-ray data for compounds **MUV-1-Br**, **MUV-1-CH$_3$** and **MUV-1-NH$_2$** were collected at a temperature of 100 K (**MUV-1-Br**, **MUV-1-NH$_2$**) or 150 K (**MUV-1-CH$_3$**) using a Rigaku FR-X rotating anode diffractometer, equipped with Hybrid Photon detector HyPix-6000HE and an Oxford Cryosystems nitrogen flow gas system.

A summary of the data collection and structure refinements is provided in Supplementary Section 2.

Optical microscopy and AFM. Optical images were obtained with a Nikon Eclipse LV-100 Optical microscope and AFM images were performed with a Nanoscope IVa multimode scanning probe microscope (Bruker) in tapping mode.

TEM. Several mechanical exfoliated flakes were transferred onto a grid with a membrane of amorphous SiN (50 nm thick) using a dry and deterministic method (involving the use of a micromanipulator and PDMS/PPC polymers, as reported in ref. [37]). TEM images and diffraction patterns were acquired with a JEOL JEM-2100F with a field-emission gun operating at 200 kV. Simulated SAED patterns were generated with SingleCrystal software.

Contact angle measurements. Static water contact angle measurements of the samples were performed in air using a Rame-hart 200 standard goniometer equipped with an automated dispensing system. The initial drop volume was 0.17 µl, which was increased by additions of 0.08 µl.

MFM. Magnetic images were recorded with a commercial LT-MFM (attoMFM I, Attocube Systems) with a commercial magnetic-coated cantilever (Nanosensors PPP-MFMR). The sample was cooled with an applied external out-of-plane field of +1 T, to assure that the tip magnetization was out of plane.

Magnetic measurements. Variable-temperature (2–300 K) direct current (d.c.) magnetic susceptibility measurements were carried out in applied fields of 1.0 kOe and variable field magnetization measurements up to ±5 T at 2.0 K. Susceptibility data were corrected from the diamagnetic contributions as deduced using Pascal's constant tables. Variable-temperature (16–23 K) alternating current (a.c.) magnetic susceptibility measurements in a ±4.0 G oscillating field at frequencies in the range of 1–997 Hz were carried out in a zero d.c. field.

Nanomechanical resonators. Suspended membranes were fabricated by exfoliating **MUV-1-Cl** flakes directly on top of circular cavities lithographically defined on a Si/SiO$_2$ substrate (SiO$_2$ thickness of 285 nm).

Laser interferometry measurements. The motion of the **MUV-1-X** mechanical resonators was measured in vacuum, using a laser interferometry set-up, similar to the one reported in ref. [35]. A modulated blue laser was used to sequentially heat up the membrane, bringing it into motion. A different, red laser was focused onto the suspended membrane and partly reflected by the membrane and partly by the silicon chip underneath. As the membrane moved, the effective cavity depth was modulated. This modulated the intensity of the reflected laser beam by interference, which was captured by a photodiode. The measurements were carried out in a homodyne detection scheme, using a vector network analyser.

Data availability. All data generated and analysed during this study are included in this Article and its Supplementary Information, and are also available from the authors upon reasonable request. Atomic coordinates and structure factors for the reported crystal structures have been deposited in the Cambridge Crystallographic Data Centre under accession codes CCDC 1582347 (**MUV-1-CH$_3$**), 1582348 (**MUV-1-H**), 1582349 (**MUV-1-NH$_2$**), 1582350 (**MUV-1-Cl**) and 1849147 (**MUV-1-Br**). Copies of the data can be obtained free of charge from www.ccdc.cam.ac.uk/structures/.

Received: 14 November 2017; Accepted: 27 June 2018;
Published online: 27 August 2018

References

1. Ferrari, A. C. et al. Science and technology roadmap for graphene, related two-dimensional crystals, and hybrid systems. *Nanoscale* **7**, 4598–4810 (2015).
2. Dean, C. R. et al. Boron nitride substrates for high-quality graphene electronics. *Nat. Nanotechnol.* **5**, 722–726 (2010).
3. Mañas-Valero, S., García-López, V., Cantarero, A. & Galbiati, M. Raman spectra of ZrS_2 and $ZrSe_2$ from bulk to atomically thin layers. *Appl. Sci.* **6**, 264 (2016).
4. Mak, K. F., Lee, C., Hone, J., Shan, J. & Heinz, T. F. Atomically thin MoS_2: a new direct-gap semiconductor. *Phys. Rev. Lett.* **105**, 136805 (2010).
5. Carvalho, A. et al. Phosphorene: from theory to applications. *Nat. Rev. Mater.* **1**, 16061 (2016).
6. Acerce, M., Voiry, D. & Chhowalla, M. Metallic 1T phase MoS_2 nanosheets as supercapacitor electrode materials. *Nat. Nanotech.* **10**, 313–318 (2015).
7. Xu, C. et al. Large-area high-quality 2D ultrathin Mo_2C superconducting crystals. *Nat. Mater.* **14**, 1135–1141 (2015).
8. El-Bana, M. S. et al. Superconductivity in two-dimensional $NbSe_2$ field effect transistors. *Supercond. Sci. Technol.* **26**, 125020 (2013).
9. Navarro-Moratalla, E. et al. Enhanced superconductivity in atomically thin TaS_2. *Nat. Commun.* **7**, 11043 (2016).
10. Hardy, W. J. et al. Thickness-dependent and magnetic-field-driven suppression of antiferromagnetic order in thin V_5S_8 single crystals. *ACS Nano* **10**, 5941–5946 (2016).
11. Lee, J.-U. et al. Ising-type magnetic ordering in atomically thin $FePS_3$. *Nano Lett.* **16**, 7433–7438 (2016).
12. Gong, C. et al. Discovery of intrinsic ferromagnetism in two-dimensional van der Waals crystals. *Nature* **546**, 265–269 (2017).
13. Huang, B. et al. Layer-dependent ferromagnetism in a van der Waals crystal down to the monolayer limit. *Nature* **546**, 270–273 (2017).
14. Diercks, C. S. & Yaghi, O. M. The atom, the molecule, and the covalent organic framework. *Science* **355**, 1585 (2017).
15. Liu, W. et al. A two-dimensional conjugated aromatic polymer via C–C coupling reaction. *Nat. Chem.* **9**, 563–570 (2017).
16. Rodríguez-San-Miguel, D., Amo-Ochoa, P. & Zamora, F. MasterChem: cooking 2D-polymers. *Chem. Commun.* **52**, 4113–27 (2016).
17. Peng, Y. et al. Metal–organic framework nanosheets as building blocks for molecular sieving membranes. *Science* **346**, 1356–1359 (2014).
18. Rodenas, T. et al. Metal–organic framework nanosheets in polymer composite materials for gas separation. *Nat. Mater.* **14**, 48–55 (2015).
19. Lahiri, N., Lotfizadeh, N., Tsuchikawa, R., Deshpande, V. V. & Louie, J. Hexaaminobenzene as a building block for a family of 2D coordination polymers. *J. Am. Chem. Soc.* **139**, 19–22 (2017).
20. Araki, T., Kondo, A. & Maeda, K. The first lanthanide organophosphonate nanosheet by exfoliation of layered compounds. *Chem. Commun.* **49**, 552–554 (2013).
21. Abhervé, A., Mañas-Valero, S., Clemente-León, M. & Coronado, E. Graphene related magnetic materials: micromechanical exfoliation of 2D layered magnets based on bimetallic anilate complexes with inserted $[Fe^{III}(acac_2\text{-trien})]^+$ and $[Fe^{III}(sal_2\text{-trien})]^+$ molecules. *Chem. Sci.* **6**, 4665–4673 (2015).
22. Foster, J. A., Henke, S., Schneemann, A., Fischer, R. A. & Cheetham, A. K. Liquid exfoliation of alkyl-ether functionalised layered metal–organic frameworks to nanosheets. *Chem. Commun.* **52**, 10474–10477 (2016).
23. Shi, W. et al. Surface modification of two-dimensional metal–organic layers creates biomimetic catalytic microenvironments for selective oxidation. *Angew. Chem. Int. Ed.* **56**, 9704–9709 (2017).
24. Peng, Y. et al. Two-dimensional metal–organic framework nanosheets for membrane-based gas separation. *Angew. Chem. Int. Ed.* **56**, 9757–9761 (2017).
25. Lei, S. et al. Surface functionalization of two-dimensional metal chalcogenides by Lewis acid-base chemistry. *Nat. Nanotech.* **11**, 465–471 (2016).
26. Gaur, A. P. S. et al. Surface energy engineering for tunable wettability through controlled synthesis of MoS_2. *Nano Lett.* **14**, 4314–4321 (2014).
27. Faghani, A. et al. Controlled covalent functionalization of thermally reduced graphene oxide to generate defined bifunctional 2D nanomaterials. *Angew. Chem. Int. Ed.* **56**, 2675–2679 (2017).
28. Rettig, S. J., Storr, A., Summers, D. A., Thompson, R. C. & Trotter, J. Transition metal azolates from metallocenes. 2. Synthesis, X-ray structure, and magnetic properties of a three-dimensional polymetallic iron(II) imidazolate complex, a low-temperature weak ferromagnet. *J. Am. Chem. Soc.* **119**, 8675–8680 (1997).

29. Lines, M. E. The quadratic-layer antiferromagnet. *J. Phys. Chem. Solids* **31**, 101–116 (1970).
30. Nguyen, L. et al. Atomic defects and doping of monolayer $NbSe_2$. *ACS Nano* **11**, 2894–2904 (2017).
31. Rooney, A. P. et al. Observing imperfection in atomic interfaces for van der Waals heterostructures. *Nano Lett.* **17**, 5222–5228 (2017).
32. Hartmann, U. Magnetic force microscopy. *Annu. Rev. Mater. Sci.* **29**, 53–87 (1999).
33. Serri, M. et al. Low-temperature magnetic force microscopy on single molecule magnet-based microarrays. *Nano Lett.* **17**, 1899–1905 (2017).
34. Zhu, X. et al. Signature of coexistence of superconductivity and ferromagnetism in two-dimensional $NbSe_2$ triggered by surface molecular adsorption. *Nat. Commun.* **7**, 11210 (2016).
35. Bunch, J. S. et al. Electromechanical resonators from graphene sheets. *Science* **315**, 490–493 (2007).
36. Castellanos-Gomez, A. et al. Single-layer MoS_2 mechanical resonators. *Adv. Mater.* **25**, 6719–6723 (2013).
37. Hermosa, C. et al. Mechanical and optical properties of ultralarge flakes of a metal–organic framework with molecular thickness. *Chem. Sci.* **6**, 2553–2558 (2015).
38. Britnell, L. et al. Strong light–matter interactions in heterostructures of atomically thin films. *Science* **340**, 1311–1314 (2013).

Acknowledgements

The authors acknowledge financial support from the European Comission (COST Action MOLSPIN CA15128, FET-OPEN 2D-INK 664878, ERC-2016-CoG 724681-S-CAGE and ERC-2018-AdG 788222 Mol-2D), the Spanish MINECO (Structures of Excellence María de Maeztu MDM-2015–0538 and Severo Ochoa SEV-2012-0267, projects CTQ2014-59209-P, CTQ2017-89528-P, MAT2017-89993-R, MAT2015-68200-C2-2-P and MAT2015-71842-P), the Generalitat Valenciana (Prometeo programme) and the VLC/Campus Program. G.M.E. thanks the Spanish MINECO for a Ramón y Cajal Fellowship. S.M.V. thanks MINECO for a predoctoral FPU grant (FPU14/04407). J.L.C. acknowledges the University of Valencia for an 'Atracció de Talent' grant. The C^2TN/IST authors acknowledge the Portuguese Foundation for Science and Technology (FCT, contract UID/Multi/04349/2013). D.D., P.G.S. and H.S.J.v.d.Z. acknowledge the support of the Netherlands Organisation for Scientific Research (NWO/OCW), as part of the Frontiers of Nanoscience (NanoFront) programme and the European Union Seventh Framework Programme under grant agreement no. 604391 Graphene Flagship. The authors thank the Spanish CRG-D1B at Institut Laue-Langevin for allocated beamtime (project CRG-2402).

Author contributions

J.L.C. and S.M.V. contributed equally to this work. J.L.C. synthetized and characterized all the materials in bulk. S.M.V. analysed the magnetic data and carried out the MFM measurements. S.M.V. performed the exfoliation and characterization of the exfoliated materials, assisted by J.L.C. I.J.V.Y. contributed to solution and refinement of the structures from single crystal data with the help of G.M.E. P.J.B. conducted the TEM studies with contributions from J.L.C. and S.M.V. J.A.R.V. performed the neutron diffraction studies. J.C.W. and B.J.C.V. performed the Mossbauer characterization. D.D., P.G.S. and H.S.J.v.d.Z. characterized the nanomechanical resonators. G.M.E. and E.C. conceived and designed the experiments. J.L.C., S.M.V., G.M.E. and E.C. prepared the manuscript. All authors commented on the manuscript.

Competing interests

The authors declare no competing interests.

Additional information

Supplementary information is available for this paper at https://doi.org/10.1038/s41557-018-0113-9.

Reprints and permissions information is available at www.nature.com/reprints.

Correspondence and requests for materials should be addressed to G.M. or E.C.

Publisher's note: Springer Nature remains neutral with regard to jurisdictional claims in published maps and institutional affiliations.